Michigan
Technological
University
1885

Michigan Technological University

Digital Commons @ Michigan Tech

Department of Physics Publications

Department of Physics

Fine-scale droplet clustering in atmospheric clouds: 3D radial distribution function from airborne digital holography

Michael L. Larsen
College of Charleston

Raymond Shaw
Michigan Technological University

Alexander Kostinski
Michigan Technological University

Susanne Glienke
Michigan Technological University

Follow this and additional works at: https://digitalcommons.mtu.edu/physics-fp

Part of the Atmospheric Sciences Commons, and the Physics Commons

Recommended Citation

Larsen, M. L., Shaw, R., Kostinski, A., & Glienke, S. (2018). Fine-scale droplet clustering in atmospheric clouds: 3D radial distribution function from airborne digital holography. *Physical Review Letters, 121*. http://dx.doi.org/10.1103/PhysRevLett.121.204501
Retrieved from: https://digitalcommons.mtu.edu/physics-fp/142

Editors' Suggestion   Featured in Physics

Fine-Scale Droplet Clustering in Atmospheric Clouds: 3D Radial Distribution Function from Airborne Digital Holography

Michael L. Larsen,[1,2,*] Raymond A. Shaw,[2,†] Alexander B. Kostinski,[2] and Susanne Glienke[2,3,4]

[1]*Department of Physics and Astronomy, College of Charleston, Charleston, South Carolina 29424, USA*
[2]*Department of Physics, Michigan Technological University, Houghton, Michigan 49931, USA*
[3]*Johannes Gutenberg University, Mainz, 55099, Germany*
[4]*Max Planck Institute for Chemistry, Mainz, 55128, Germany*

The extent of droplet clustering in turbulent clouds has remained largely unquantified, and yet is of possible relevance to precipitation formation and radiative transfer. To that end, data gathered by an airborne holographic instrument are used to explore the three-dimensional spatial statistics of cloud droplet positions in homogeneous stratiform boundary-layer clouds. The three-dimensional radial distribution functions $g(r)$ reveal unambiguous evidence of droplet clustering. Three key theoretical predictions are observed: the existence of positive correlations, onset of correlation in the turbulence dissipation range, and monotonic increase of $g(r)$ with decreasing r. This implies that current theory captures the essential processes contributing to clustering, even at large Reynolds numbers typical of the atmosphere.

Collections of dense particles residing in a turbulent fluid are ubiquitous in natural and applied systems, from dust in the interstellar medium, to droplets in a cloud, to fuel spray in a combustion chamber. The spatial distribution of such particles is relevant to processes such as collision rates and radiative transfer, and therefore can influence rates of planetessimal or rain formation, and the optical properties of clouds relevant to the albedo of planets [1–4].

Studies over the last two decades have shown that dense particles in a turbulent fluid tend to cluster [5–19]. More explicitly, extensive study has resulted in the following physical picture: spatial correlations between particles (1) are positive in sign, i.e., particles tend to cluster in common regions of the turbulent flow, (2) have clustering that is observed within the dissipative range of turbulence, beginning at scales of order 1–10 times the Kolmogorov length scale, and (3) have a correlation strength that increases monotonically with decreasing separation distance (as a power law).

The physical picture above is based on the simplest, limiting scenario of small particle inertia, a large particle-to-fluid density ratio, a particle diameter much less than the dissipation scale of the turbulence, no particle-particle interactions, monodisperse uniform particles, no gravitational settling or other uniform drift speeds, and the existence of fully-developed steady-state turbulence.

More recent work has attempted to determine whether the physical picture changes if some of the assumptions in this limiting scenario are relaxed. Theoretical work has examined the impact of including polydisperse particles and including a uniform drift [15,19–21], and careful laboratory observations have shown that spatial correlations are (as expected) suppressed in the presence of gravitational sedimentation or polydispersity in the particle Stokes number [22–27].

A central question that remains centers on scale dependence, which is of practical interest in geophysical and astrophysical systems: Does particle clustering in simulations and laboratory experiments with maximal spatial extents less than a meter translate quantitatively to systems such as atmospheric clouds with scales of kilometers, or to astrophysical systems with vastly larger scales? This is essentially a question of Reynolds number (Re) dependence, because of the implicit dependence on the energy-injection length scale L: $\mathrm{Re}^{3/4} \sim L/\eta$ with η the Kolmogorov length scale. Typical laboratory and simulation scale ratios reach order $L/\eta \approx 10^3$, whereas $L/\eta \approx 10^6$ and above are of interest for rain or planet formation. Turbulence is known to become strongly intermittent in the distribution of acceleration and energy dissipation with increasing Re [28,29], and because inertial clustering is a dissipation-scale phenomenon the Re dependence is open to debate.

Because systems with such wide ranges of length scales are currently out of reach of simulation and most laboratory capabilities, this study presents direct, three-dimensional measurements of in-cloud particle spatial correlations using an airborne digital-holographic instrument. While the realities of limited sampling statistics due to lack of statistical homogeneity in atmospheric flows and broad particle size distributions make a quantitative comparison to theory quite challenging at this stage, we are able to search for the three general characteristics of inertial clustering described in the first paragraph at Reynolds numbers inaccessible via other means. The results can then

be assessed for their relevance to problems such as rain formation rate or cloud albedo modification through pollution or even geoengineering.

In situ atmospheric measurements have been used to estimate several metrics of cloud particle clustering (see, e.g., Refs. [30–39]), but here we focus on the radial distribution function $g(r)$ because of its direct link to the theoretical developments previously described. Empirically, $g(r)$ reports the ratio between the observed joint probability of finding two particles with centers separated by distance $r \pm dr/2$ and the theoretical joint probability of finding two particles with centers separated by distance $r \pm dr/2$ in a Poisson distribution with the same volume and number of particles as measured. Mathematically,

$$g(r) = \sum_{i=1}^{N} \frac{\psi_i(r)/N}{(N-1)(\frac{dV_r}{V})} \qquad (1)$$

where $\psi_i(r)$ is a count of the number of particles having their centers a distance between $r - dr/2$ and $r + dr/2$ from the center of the ith particle in the measurement volume. N is the total number of particles in the measurement volume V, and dV_r is the volume of the generalized n-dimensional shell between radii $r - dr/2$ and $r + dr/2$.

When no particle pairs are found with separation $r \pm dr/2$, $g(r) = 0$. When $g(r)$ exceeds 1 for some value of r, this implies that there are more particle pairs with separations at spatial scale r than would be expected in a Poisson distribution with the same total number of particles distributed throughout the same volume (indicating spatial clustering on this scale).

The rest of this Letter (i) addresses the question of statistical confidence to identify a minimum critical spatial scale for estimation of $g(r)$, (ii) presents (to our knowledge, the first ever) *in situ* three-dimensional $g(r)$ curves for spatial scales larger than the critical spatial scale, and (iii) discusses the broader implications of these $g(r)$ observations as they relate to our understanding of cloud microphysical processes.

In order to reliably estimate $g(r)$ from cloud measurements and to identify signatures of inertial clustering, it is crucial to use a measurement strategy that allows the dissipation range to be reached with statistical significance. Because for cloud turbulence $\eta \approx 1$ mm, we desire some means of estimating $g(r)$ on mm scales. We use two strategies to accomplish this measurement challenge: First, we adopt digital holography, which allows for a three-dimensional sample volume and, as shown later, minimizes sampling uncertainty relative to more common one-dimensional sampling instruments. Second, we sample from clouds that appear statistically homogeneous in space so that multiple samples can be averaged.

Specifically, we utilize the HOLODEC (Holographic Detector for Clouds) instrument, which was deployed during the CSET (Cloud System Evolution in the Trades) experiment [40]. The CSET field campaign occurred during July and August, 2015. This experiment utilized the NSF/NCAR GV HIAPER aircraft [41] outfitted with a large number of instruments [42] for measuring thermodynamic, radiative, and cloud properties. The primary aim of CSET was to sample the transition of marine stratocumulus to trade wind cumulus clouds, making it ideal for the present study due to the occasional long continuous sampling of stratocumulus decks at constant altitude. HOLODEC is an in-line digital holography instrument explicitly designed to explore cloud microstructure [43–45]. The instrument has previously been used to examine drop size distribution and liquid water content fluctuations on the centimeter scale [46], and the behavior of the instrument during CSET has been validated by comparison to co-collected cloud data in different parts of the particle size domain [47].

This study uses HOLODEC data from four intervals during two of the CSET research flights. The four flight intervals were chosen based on (1) their nearly constant flight altitude, (2) continuous or nearly continuous collection of holograms that meet the sampling criteria of 10-μm minimum droplet size and 100-particle minimum per sample volume, and (3) having a relatively stationary drop number concentration throughout the interval. Hologram-by-hologram drop numbers, mean drop sizes, and size distributions for each of the four flight intervals are shown in the Supplemental Material [48]. HOLODEC takes images at a frequency of 3.3 Hz, so at nominal flight speeds of 136 m/s, consecutive holograms are located approximately 40 m apart from each other. In an effort to ensure that only reliable data are used, this Letter focuses on the analysis of detected particles larger than 10 μm in diameter located within a 3.6 cm^3 subvolume of each hologram. More complete information associated with the CSET HOLODEC data set and considerations related to subvolume selection can be found in Refs. [47,49].

Details about the four intervals selected are presented in Table I. For each flight interval, estimates of the turbulence energy dissipation rate (ε), mean-interval St (τ_p/τ_k relating particle inertial response time to Kolmogorov time scale) and Sv (v_t/v_η relating terminal fall speed to Kolmogorov velocity scale) were obtained by combining HOLODEC data with 25-Hz flight data [50]. The ε was computed by estimating the magnitude of the flat-portion of the second order compensated structure function of the GPS-corrected vertical velocity component of the wind. The St and Sv were estimated by using the mean measured cloud drop diameter, estimated value of ε, and other locally measured thermodynamic variables from the 25-Hz flight data, as described elsewhere [51].

We now consider the question of sampling uncertainty versus spatial scale r. Assuming statistical homogeneity over the 3.6 cm^3 sampling volume of an individual hologram, the uncertainty in the evaluation of $g(r)$ for a single

TABLE I. Summary information for flight intervals used in this study. As noted in the text, particles less than 10 μm in diameter and holograms with fewer than 100 retained droplets in the sample volume were discarded. The final four columns indicate mean interval-averaged or -estimated values of retained droplet diameter, turbulent energy dissipation rate, Stokes number, and Settling parameter. Flight interval-averaged standard deviations for droplet diameter, St, and Sv are presented in the Supplemental Material [48].

Interval ref	Flight date	Time interval (UTC)	Analyzed holograms	Retained droplets	$\langle D \rangle$ (μm)	ε (m^2/s^3)	St	Sv
A	7 July 2015	16:19–16:31	1438	459 189	15.0	9.9×10^{-4}	5.5×10^{-3}	0.61
B	7 July 2015	17:15–17:26	2005	2 014 146	15.0	1.2×10^{-3}	6.1×10^{-3}	0.59
C	27 July 2015	16:31–16:41	1835	888 511	16.0	2.7×10^{-3}	1.0×10^{-2}	0.54
D	27 July 2015	17:20–17:27	1278	346 550	20.2	1.6×10^{-3}	1.3×10^{-2}	0.99

hologram is solely driven by sampling variability, which depends on (1) the size and shape of the sample volume, (2) the scale of interest r, and (3) the number of particles in the hologram N. Since sampling uncertainty is related to shot noise in counting statistics, the uncertainty in $g(r)$ increases with decreasing r (as a spherical shell has $dV \propto r^2 dr$). Further, there is substantial hologram to hologram variability in the number of cloud particles present (e.g., see figure in the Supplemental Material [48]).

To illustrate, we consider an example that highlights the influence of particle number and sampling volume shape (see table in Supplemental Material [48] for more details). A 3D volume matching the size and shape of the HOLODEC sample volume is compared to a 1D volume matching that sampled by a single-drop counting instrument (like a Forward Scattering Spectrometer Probe [34]) sampling an equivalent 3.6 cm^3 volume. The cloud droplet concentration is chosen as either 70 cm^{-3} or 300 cm^{-3} (approximately the range of values seen in the four flight intervals in this study). The values of r and dr chosen are the same ones used in the rest of this study.

To estimate the uncertainty in $g(r)$, we use an *ad hoc* method designed to quantify the plausible sampling variability. If $\mathcal{N}$ is the number of observed particle pairs separated by $r \pm dr/2$ and $\mathcal{P}$ is the number of expected particle pairs separated by $r \pm dr/2$ in a Poisson distribution with the same number of particles, then we know $g_{\text{meas}}(r) = \mathcal{N}/\mathcal{P}$. We define

$$g^{\pm}(r) \equiv \frac{\mathcal{N} \pm \sqrt{\mathcal{N}}}{\mathcal{P} \mp \sqrt{\mathcal{P}}} \qquad (2)$$

using the assumption that the uncertainty in $\mathcal{N}$ and $\mathcal{P}$ scale as $\mathcal{N}^{1/2}$ and $\mathcal{P}^{1/2}$ (counting variables), respectively. For a measured $g_{\text{meas}}(r)$, the true intrinsic value of $g(r)$ likely lies between $g^-(r)$ and $g^+(r)$.

Figure 1 shows regions bounded by $g^-(r)$ and $g^+(r)$ as a function of r when $\mathcal{N} = \mathcal{P}$; these are *calculated* curves (not corresponding to simulation or real data) that demonstrate the uncertainty due to sampling statistics only. Though $g(r) \equiv 1$ by construction, a measurement of $g(r)$ could potentially end up anywhere in the gray-shaded region.

The figure clearly demonstrates that using a fully 3D measurement allows access to the mm-scale range by diminishing the sampling uncertainty for a single holo-gram. Specifically, HOLODEC sample volumes can be used to measure $g(r)$ on scales larger than $\sim$1 mm, thereby allowing the onset of the dissipation range to be examined. These sampling considerations, along with consideration of
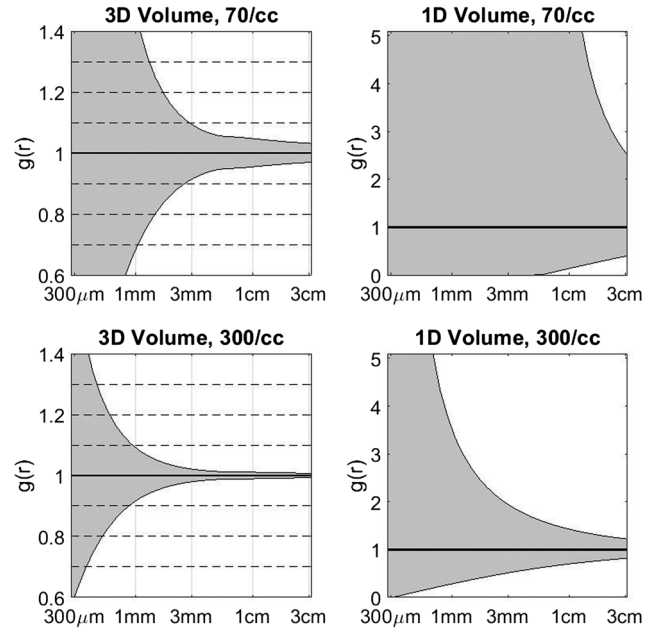

FIG. 1. Quantifying the uncertainty due to counting statistics in the estimation of $g(r)$ as a function of scale for differently shaped volumes and realistic cloud droplet concentrations. Each panel shows a range where the measured $g(r)$ might lie when the intrinsic system $g(r)$ is known to be unity. These curves are derived from applying $\sqrt{N}$ uncertainty estimates to the counting statistics needed to compute $g(r)$. The 3D volumes match the aspect ratio of the HOLODEC sample volume, while the 1D volumes are designed to mimic a typical single-particle-counting instrument viewing the same total volume. Note that the scale of the 1D volume panels had to be magnified, since the uncertainty is many times larger for 1D data sets. Individual hologram $g(r)$ estimates for HOLODEC data drop below 10% uncertainty for spatial scales somewhere between 1 and 3 mm, depending on droplet number concentration.
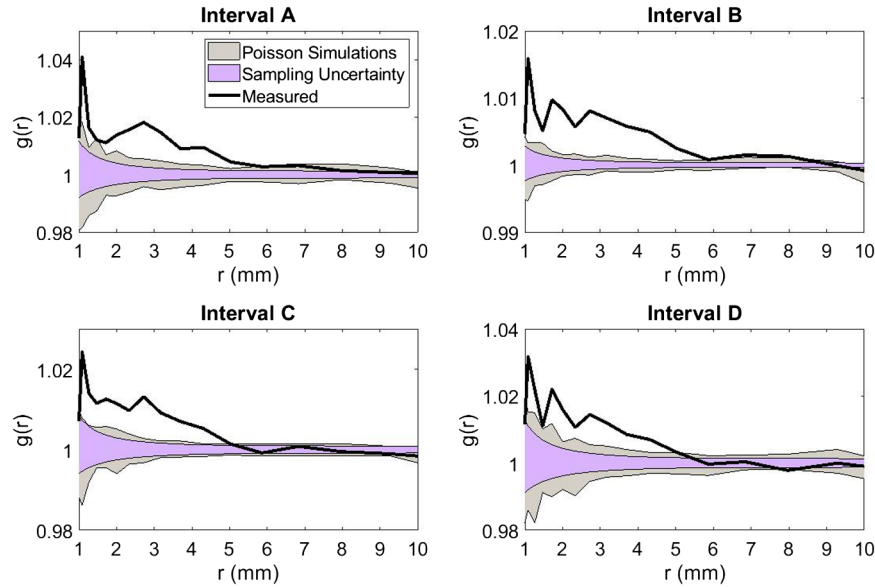
FIG. 2.   The interval-averaged radial distribution functions for each of the four flight intervals examined in this study. The observed radial distribution functions exceed the maximum value expected based on sampling uncertainty throughout the range 1–5 mm in all flight intervals. Three key theoretical predictions are observed: positive correlation, onset of correlation in the dissipation range (less than approximately 10 mm), and monotonic increase of $g(r)$ with decreasing r. The two shaded regions quantify the sampling uncertainty via two independent methods explained in the text.

instrument inhomogeneities (see Supplemental Material [48] for details), motivate averaging $g(r)$ from multiple holograms to reduce sampling uncertainty.

Figure 2 shows the interval-averaged radial distribution functions for the four flight intervals. In addition to plotting the flight-interval averaged $g(r)$ (solid black curve), two separate regions are marked to quantify the interval-averaged uncertainty. The pale maroon shading is found by extending the single-hologram uncertainty results shown in the left panels of Fig. 1 to an entire flight interval. Essentially, the thickness of the envelope is scaled by $N_h^{-1/2}$ where N_h is the number of holograms in the interval. The gray shading is determined through Monte Carlo sampling from 100 simulants of each flight interval. For each simulant a sequence of holograms with the same number of particles per hologram as the underlying flight intervals was created. All particles were placed in each simulated hologram's $6 \text{ mm} \times 6 \text{ mm} \times 10 \text{ cm}$ spatial domain perfectly randomly. For each of the 100 simulants, the mean $g(r)$ was computed; all 100 simulant mean $g(r)$ curves lie within the gray region in Fig. 2.

The two independent methods for determining sampling uncertainty allow us to conclude that the measured $g(r)$ show statistically significant clustering of cloud droplets in the range of approximately 1–5 mm. We observe that the measured $g(r)$ are consistent with the three core predictions of the theory of inertial-particle clustering in turbulence. Namely, (1) the spatial correlations between particles are positive in sign, (2) clustering is observed within the dissipative range of turbulence, beginning at lengths of

order 10η, and (3) the correlation strength increases monotonically with decreasing separation distance. Regarding the third point, the theory predicts power-law behavior, but the accessible range of scales is too limited to allow a reliable conclusion in that regard (although the curves are at least qualitatively consistent with power-law-like behavior). The consistency with this theoretical picture suggests that other mechanisms not accounted for in the theory, such as particle charge and microhydrodynamic interactions, are not playing a strong role at the measured scales. Because of the large length and time scales typical of atmospheric flows, the measurements also suggest that clustering behavior does not change drastically at large Reynolds numbers.

It is worth emphasizing that the requirement of averaging over multiple holograms, which required that we sample in a stratocumulus environment, places us in conditions least favorable to detect cloud droplet inertial clustering. Isolated convective clouds have much higher turbulence energy dissipation rates and therefore tend to favor higher Stokes numbers and lower settling parameters [51]. Theory and computation suggest that the shape and the magnitude of the radial distribution function in a turbulent environment is related to the intensity of the ambient turbulence (see, e.g., Refs. [5,15,18,20,21]). Indeed, the flight-interval averaged clustering has signals of the same order of magnitude as those observed in the laboratory at lower Reynolds numbers, for realistic particle size distributions [27].

If small $g(r)$ values are common in the atmosphere, it may help to understand why earlier, smaller-scale studies of

atmospheric particulate clustering using holographic measurements [32,52–55] gave somewhat conflicting results; it was only due to the large amounts of data available in this study that the sampling variability could be lowered enough to get an unambiguous confirmation of weak clustering. With less data, our results—like many of those in the studies before ours—would have been inconclusive.

In summary, holographic measurements have led to the first fully three-dimensional radial distribution functions from in-cloud droplet spatial positions. Sampling considerations require subtle consideration of the observed radial distribution functions, but a simple argument based on instrumental and physical parameters showed that there exists a critical spatial scale (∼1 mm) above which data from the HOLODEC instrument can be reliably used in realistic cloud conditions to estimate the radial distribution function. Analysis of this radial distribution function from four distinct flight-intervals during CSET revealed statistically significant and unambiguous evidence of weak clustering on scales between about 1 and 5 mm. The measurements are consistent with three key predictions of the theory: positive spatial correlations, onset in the dissipation range of the turbulent flow, and monotonic increase with decreasing spatial scale. Though these clustering signals are small for these weakly turbulent clouds, the ability to validate the existing theoretical picture, even at a semiquantitative level, suggests that the theory can be extended to other conditions encountered in the atmosphere.

[*]LarsenML@cofc.edu
[†]rashaw@mtu.edu

[1] J. Cuzzi, R. Hogan, J. Paque, and A. Dobrovolskis, Astrophys. J. **546,** 496 (2001).
[2] R. Shaw, Annu. Rev. Fluid Mech. **35,** 183 (2003).
[3] K. Gustavsson and B. Mehlig, Eur. Phys. J. E **39,** 55 (2016).
[4] A. Pumir and M. Wilkinson, Annu. Rev. Condens. Matter Phys. **7,** 141 (2016).
[5] W. Reade and L. Collins, Phys. Fluids **12,** 2530 (2000).
[6] L.-P. Wang, A. Wexler, and Y. Zhou, J. Fluid Mech. **415,** 117 (2000).
[7] E. Balkovsky, G. Falkovich, and A. Fouxon, Phys. Rev. Lett. **86,** 2790 (2001).
[8] Y. Zhou, A. Wexler, and L.-P. Wang, J. Fluid Mech. **433,** 77 (2001).
[9] G. Falkovich, A. Fouxon, and M. Stepanov, Nature (London) **419,** 151 (2002).
[10] J. Bec, Phys. Fluids **15,** L81 (2003).
[11] L. Zaichik and W. Alipchenkov, Phys. Fluids **15,** 1776 (2003).
[12] G. Falkovich and A. Pumir, Phys. Fluids **16,** L47 (2004).
[13] B. Mehlig and M. Wilkinson, Phys. Rev. Lett. **92,** 250602 (2004).
[14] J. Bec, A. Celani, M. Cencini, and S. Musacchio, Phys. Fluids **17,** 073301 (2005).
[15] J. Chun, D. Koch, S. Rani, A. Ahluwalia, and L. Collins, J. Fluid Mech. **536,** 219 (2005).
[16] M. Wilkinson and B. Mehlig, Europhys. Lett. **71,** 186 (2005).
[17] L. Zaichik and W. Alipchenkov, Phys. Fluids **19,** 113308 (2007).
[18] P. Ireland, A. Bragg, and L. Collins, J. Fluid Mech. **796,** 617 (2016).
[19] P. Ireland, A. Bragg, and L. Collins, J. Fluid Mech. **796,** 659 (2016).
[20] J. Bec, H. Homann, and S. S. Ray, Phys. Rev. Lett. **112,** 184501 (2014).
[21] K. Gustavsson, S. Vajedi, and B. Mehlig, Phys. Rev. Lett. **112,** 214501 (2014).
[22] J. Salazar, J. D. Jong, L. Cao, C. Woodward, H. Meng, and L. Collins, J. Fluid Mech. **600,** 245 (2008).
[23] E.-W. Saw, R. Shaw, S. Ayyalasomayajula, P. Chuang, and A. Gylfason, Phys. Rev. Lett. **100,** 214501 (2008).
[24] J. Lu, H. Nordsiek, and R. Shaw, New J. Phys. **12,** 123030 (2010).
[25] H. Siebert, S. Gerashchenko, A. Gylfason, K. Lehmann, L. Collins, R. Shaw, and Z. Warhaft, Atmos. Res. **97,** 426 (2010).
[26] C. Bateson and A. Aliseda, Exp. Fluids **52,** 1373 (2012).
[27] E.-W. Saw, R. Shaw, J. Salazar, and L. Collins, New J. Phys. **14,** 105031 (2012).
[28] J. C. Wyngaard, Annu. Rev. Fluid Mech. **24,** 205 (1992).
[29] K. Sreenivasan and R. Antonia, Annu. Rev. Fluid Mech. **29,** 435 (1997).
[30] B. Baker, J. Atmos. Sci. **49,** 387 (1992).
[31] D. Baumgardner, B. Baker, and K. Weaver, J. Atmos. Ocean. Technol. **10,** 557 (1993).
[32] E.-M. Uhlig, S. Borrmann, and R. Jaenicke, Tellus **50,** 377 (1998).
[33] A. Kostinski and A. Jameson, J. Atmos. Sci. **57,** 901 (2000).
[34] L. Chaumat and J. Brenguier, J. Atmos. Sci. **58,** 642 (2001).
[35] A. Kostinski and R. Shaw, J. Fluid Mech. **434,** 389 (2001).
[36] M. Pinsky and A. Khain, J. Appl. Meteorology **40,** 1515 (2001).
[37] R. Shaw, A. Kostinski, and M. Larsen, Q. J. R. Meteorol. Soc. **128,** 1043 (2002).
[38] Y. Knyazikhin, A. Marshak, M. Larsen, W. Wiscombe, J. Martonchik, and R. Myneni, J. Atmos. Sci. **62,** 2555 (2005).
[39] A. Marshak, Y. Knyazikhin, M. Larsen, and W. J. Wiscombe, J. Atmos. Sci. **62,** 551 (2005).
[40] B. Albrecht, V. Ghate, J. Mohrmann, R. Wood, P. Zuidema, C. Bretherton, C. Schwartz, E. Eloranta, S. Glienke, S. Donaher, M. Sarkar, J. McGibbon, A. Nugent, R. Shaw, J. Fugal, P. Minnis, R. Paliknoda, L. Lussier, J. Jensen, J. Vivekanandan et al., Bull. Am. Meteorological Society, DOI: 10.1175/BAMS-D-17-0180.1 (2018).

[41] UCAR/NCAR-Earth Observing Laboratory, "Nsf/ncar gv hiaper aircraft" (2005), DOI: 10.5065/D6DR2SJP.

[42] UCAR/NCAR-Earth Observing Laboratory, "Low rate (lrt-1 sps) navigation, state parameter, and microphysics flight-level data, version 2.0"(2017), DOI: 10.5065/D65Q4T96.

[43] J. Fugal, R. Shaw, E.-W. Saw, and A. Sergeyev, Appl. Opt. **43**, 5987 (2004).

[44] J. Fugal and R. Shaw, Atmos. Meas. Tech. **2**, 259 (2009).

[45] S. Spuler and J. Fugal, Appl. Opt. **50**, 1405 (2011).

[46] M. Beals, J. Fugal, R. Shaw, J. Lu, S. Spuler, and J. Stith, Science **350**, 87 (2015).

[47] S. Glienke, A. Kostinski, J. Fugal, R. Shaw, S. Borrmann, and J. Stith, Geophys. Res. Lett. **44**, 8002 (2017).

[48] See Supplemental Material at http://link.aps.org/supplemental/10.1103/PhysRevLett.121.204501 for additional details about instrument, data, and analysis.

[49] M. Larsen and R. Shaw, Atmos. Meas. Tech. **11**, 4261 (2018).

[50] UCAR/NCAR-Earth Observing Laboratory, "High rate (hrt—25 sps) navigation, state parameter, and microphysics flight-level data, version 2.0" (2017), DOI: 10.5065/D63R0R3W.

[51] H. Siebert, R. Shaw, J. Ditas, T. Schmeissner, S. Malinowski, E. Bodenshatz, and H. Xu, Atmos. Meas. Tech. **8**, 3219 (2015).

[52] B. Conway, S. Caughey, A. Bentley, and J. Turton, Atmospheric Environment **16**, 1193 (1982).

[53] A. Kozikowsa, K. Haman, and J. Supronowicz, Q. J. R. Meteorol. Soc. **110**, 65 (1984).

[54] P. Brown, J. Atmos. Ocean. Technol. **6**, 293 (1989).

[55] S. Borrmann, R. Jaenicke, and P. Neumann, Atmos. Res. **29**, 229 (1993).